

VICTORIA UNIVERSITY
MELBOURNE AUSTRALIA

Light conducting photocatalytic membrane for chemical-free fouling control in water treatment

This is the Published version of the following publication

Nyamutswa, Lavern Tendayi, Zhu, Bo, Collins, Stephen F, Navaratna, Dimuth and Duke, Mikel (2020) Light conducting photocatalytic membrane for chemical-free fouling control in water treatment. *Journal of Membrane Science*, 604. ISSN 0376-7388

The publisher's official version can be found at
<https://www.sciencedirect.com/science/article/pii/S0376738820305974?via%3Dihub>
Note that access to this version may require subscription.

Downloaded from VU Research Repository <https://vuir.vu.edu.au/41206/>

Light conducting photocatalytic membrane for chemical-free fouling control in water treatment

Lavern T. Nyamutswa ^a, Bo Zhu ^a, Stephen F. Collins ^b, Dimuth Navaratna ^{a, b} and Mikel C. Duke ^{a, *}

^a *Institute for Sustainable Industries and Liveable Cities, Victoria University, Melbourne, Australia*

^b *College of Engineering and Science, Victoria University, Melbourne, Australia*

* *Corresponding author: Mikel C. Duke (email: mikel.duke@vu.edu.au)*

Abstract

This work shows for the first time the convenient *in-situ* UV illumination of a titanium dioxide (TiO₂) photocatalytic membrane via a porous glass substrate for effective fouling reduction during water treatment. By directing light through the light conducting substrate, this concept overcomes the current challenge of photocatalytic membranes that direct light through turbid, light obstructing feed waters. The effect was demonstrated on an immobilised TiO₂ membrane fabricated on sintered porous glass. Fouling was tested by filtering model solutions of humic acid (HA), bovine serum albumin (BSA) or sodium alginate (SA). Photocatalysis initiated by simply directing light via the permeate side through the porous glass substrate led to significant reductions in trans-membrane pressure (TMP) rise rates between backwashes and all model organic fouling compounds. Specifically, the UV-light exposed membranes showed a 3.0-fold and 2.4-fold reduction in total filtration resistance for BSA and SA solutions, respectively, which also showed 2.7-fold and 4.2-fold reductions in the irreversible fouling indices. Analysis by SEM coupled with fouling modelling showed the beneficial photocatalytic effects stemmed from reduced intrusion of organic material inside the TiO₂ membrane pores, as well as reduced cake layer resistance. The novel, convenient light conducting photocatalytic membranes concept could be used for sustainable, low-chemical membrane filtration of polluted water.

Keywords

membrane fouling, photocatalytic membrane, self-cleaning, water treatment

Highlights

A light conducting photocatalytic membrane is fabricated from sintered glass and TiO₂.

Light to the photocatalyst is directed through the substrate, instead of the feed stream.

Up to 4.2 -fold reduction in total filtration resistances and irreversible fouling indices.

Novel concept could utilise solar energy to significantly offset maintenance chemicals.

1. Introduction

Membrane filtration processes are an attractive solution to pathogen and contaminant removal in water because of their proven effectiveness even at low contaminant concentrations [1] to meet water quality standards and guidelines [2, 3]. However, since membranes only provide a barrier for separation of contaminants from water, disposing of the separated waste generated from the process becomes a new challenge. Membrane fouling is also a major drawback which reduces separation efficiency, permeate flux [4], membrane lifespan [5] and increases transmembrane pressure (TMP) required to maintain flux and necessitates more frequent chemical cleaning [6]. Adopting a method to minimise or reverse membrane fouling is the reality of all membrane processes. Researchers continue to study membrane fouling as they consider this is a very complex and challenging task. The water treatment industry believes that modern research studies could contribute to minimisation and control of membrane fouling, allowing the wider adoption of membrane technology.

Membrane anti-fouling techniques such as chemical, hydraulic, physical or electrical cleaning of the membrane pose undesirable elements to the process such as downtime, increased running costs and inflicting damage to the membrane. Chemical cleaning in particular gives rise to the need for purchasing of chemicals, transportation and safe storage, followed by correct use and handling, which requires some level of expertise, and their eventual safe disposal. All these come at a significant cost which increases the price of treated water. In some communities such as rural and remote areas, membrane chemical cleaning, and thus membrane water treatment, is not a viable option because of a lack of the required resources.

To address these challenges, photocatalysis could be adopted to improve the filtration performance of membranes as an *in-situ* method of fouling management. By immobilising heterogeneous semiconductor photocatalysts such as titanium dioxide (TiO₂) on the membrane surface, the separation function of membranes and the oxidative degradation ability of photocatalysts could be combined into one unit to give a superior hybrid membrane material [7]. As the membrane separates the targeted water contaminants, the photocatalyst degrades them into non-harmful, smaller molecules [8], which has a double-edged positive effect. Firstly, the degradation as well as photocatalytically induced super-hydrophilicity prevents accumulation of the contaminants on the membrane surface and hence, contributes to resolving the excessive fouling of the membrane and enable high flux/low pressure performance. Secondly, by preventing the accumulation of foulants on the membrane, the secondary waste disposal problem from using maintenance cleaning chemicals would be avoided. Such hybrid membranes are aptly dubbed “self-cleaning”, in that they continuously regenerate themselves without the need to apply some external cleaning method [5].

Also occurring simultaneously with oxidative degradation to reduce membrane fouling is induced super-hydrophilicity. In this phenomenon, radiation energy provided by an energy source results in the creation of electron-hole pairs on the TiO₂ photocatalyst coated membrane surface. The photo-generated hole then weakens the bond between titanium and the lattice oxygen atom, resulting in it being broken by water adsorbed to the membrane surface to form new Ti–OH bonds [9]. These new hydroxyl groups on the membrane surface induce super-

hydrophilicity, which prevents hydrophobic compounds from attaching to the membrane, thus keeping it free from foulants.

Photocatalytic membrane technology, however, also consists of a significant number of challenges. To start with, for the photocatalytic process to be activated, light of the correct wavelength needs to be supplied to the membrane surface at sufficient intensities [10]. One of the main challenges which is of interest in membrane photocatalysis is how to supply this light to the photocatalyst. Ever since the photocatalytic membrane was developed, the traditional approach to deliver light to the membrane was to transmit light through the contaminated water being treated. This approach is a recognised operational challenge in photocatalytic membrane technology, because of the high propensity of light to be absorbed and scattered by the water contaminants before the light rays reach the photocatalyst coated active layer of the membrane. This becomes an even more significant challenge in turbid waters where such light attenuation considerably reduces the efficiency of the photocatalytic process [11].

Having recognised this challenge, Starr *et al.* [11] adopted a novel approach of immobilising the photocatalyst onto the membrane's substrate support side instead of the functional active layer, as shown Figure S1. The main motivation in this approach was to deliver light through the permeate, which is less turbid, and therefore, results in less light scattering. Even though this method combines the separation ability of a membrane and degradation function of photocatalysis, the processes occur on different surfaces, and hence the anti-fouling ability of photocatalysis does not exist in this membrane separation configuration.

Horovitz *et al.* [12] also attempted an alternative method of delivering light by directing it from the permeate stream, with the membrane prepared in the traditional way of immobilising the photocatalyst on the membrane separation layer. In this approach, water flows from the substrate, non-functional side of the membrane, meaning that it can reach the photocatalytic layer when it is still significantly contaminated. The schematic of their approach is shown in Figure S2. While both cases showed potential by harnessing the cleaner permeate side to better facilitate the introduction of UV light to the membrane, they still do not conform to the traditional well-known format of high performance membranes involving raw water being fed directly to the selective layer with inbuilt anti-fouling functionality.

In this study, we proposed a novel alternative approach to overcome the challenges of directing light from the source to the photocatalyst coated active layer of the membrane via a light conducting substrate. This concept was previously demonstrated and validated by our research group in *ex-situ* tests [13]. By adopting this configuration in which light is directed from the end of an element through the membrane substrate, the nature of water being treated becomes a less significant factor in determining the efficiency of the photocatalytic process than in current configurations. The previous results confirmed that light could be directed successfully through the substrate to achieve a photocatalytic effect on the membrane surface. The preliminary experiments also showed that the configuration could be adopted for *ex-situ* control of membrane fouling. However, an *in-situ* demonstration within the industry-standard pressurised dead-end membrane filtration (with backwashing) format is clearly needed for the practical implementation of this concept. The working principle is depicted in Figure 1. In this

article, this novel approach is demonstrated for the first time as an effective strategy for *in-situ* control of membrane fouling.

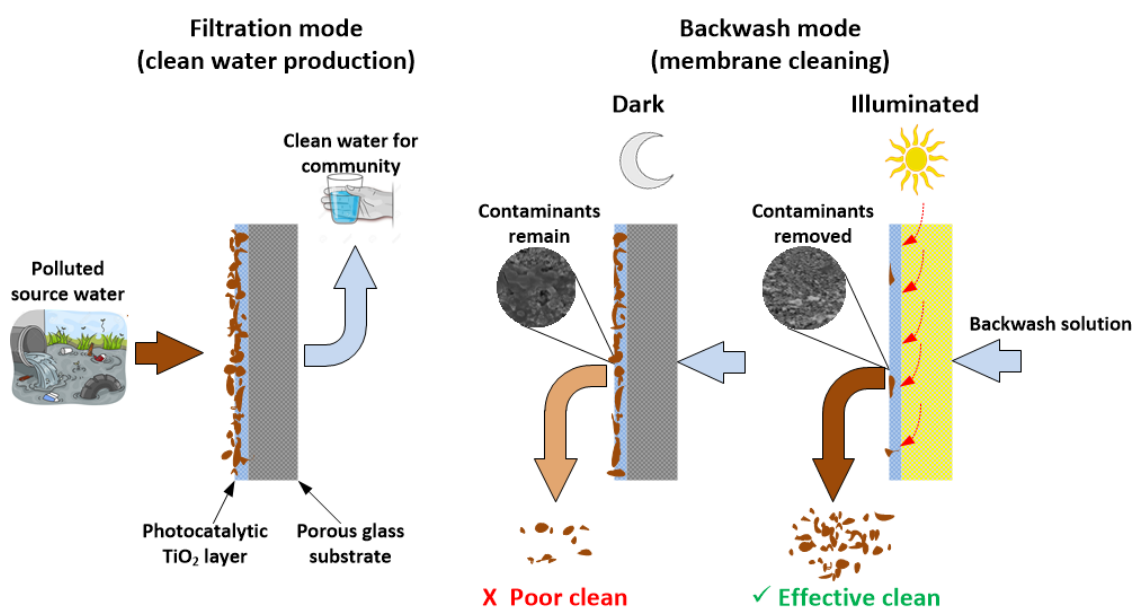


Figure 1. Chemical-free fouling management by illuminating light-conducting photocatalytic membrane with a light source.

The impact of organics on membrane performance was considered as the basis for measuring beneficial effects from the photocatalytic action. Model solutions of typical organic water contaminants were filtered through the membrane to observe anti-fouling and separation behaviour. In this study, three types of organic compounds found in water were used. These are humic acid (HA), as a representative of humic substances, sodium alginate (SA), representing polysaccharides and bovine serum albumin (BSA), a common water-borne protein. Apart from being undesirable water contaminants [14] these three groups of organic compounds were specifically chosen because they are known to be chiefly responsible for irreversible fouling in membrane water treatment [15].

2. Experimental

2.1. Materials

Analytical grade chemicals were used in the experiments. NaOH (Fischer Scientific, Loughborough, UK) and NaOCl (Sigma Aldrich, St. Louis, MO, USA) were used to prepare solutions for chemical cleaning of membrane substrates.

NaCl (Ajax Finechem, Scoresby, Australia) and CaCl₂ (Sigma Aldrich, St. Louis, MO, USA) were used to add ions to synthetic water contaminant solutions. Ions were added to synthetic contaminated water to mimic the ionic load in surface/ground water. HA (Fluka AG Cheische Fabrik., Buchs, Switzerland) was used as a representative natural organic matter (NOM) water

contaminant. BSA (Sigma Aldrich, St. Louis, MO, USA) of average molecular weight 66 kDa was used as a representative protein water contaminant. SA (Ajax Chemicals, Melbourne, Australia) was used as a representative polysaccharide water contaminant as well as a binder in the preparation of membranes.

TiO₂ P25 nanoparticles with 99.8% purity and a composition of 80% anatase and 20% rutile phases, average particle size of 30 nm and a specific surface area of 50 m²/g were acquired from Degussa AG, Frankfurt, Germany. When dispersed in water, the hydrodynamic size of P25 particles is known to increase from a few nanometres up to 300 nm [16, 17]. Sintered glass discs of 25 mm diameter, 2 mm thickness and G5 porosity were sourced from Ningbo Ja-Hely Technology Co., Ltd., Ningbo, China.

2.2. Apparatus and equipment

A sonic bath (Soniclean 500HT, Transtek Systems, Melbourne, Australia) was used to enhance membrane cleaning before the TiO₂ coating was applied, as well as for removing air bubbles and break aggregates in the coating suspension. A fan forced oven (S.E.M Equipment, Australia) was used for drying wet membranes after dip coating. A programmable Vulcan 3-550PD NEY furnace (Extech Equipment, Victoria, Australia) was used for sintering the membranes after coating and drying. During filtration, the membrane was placed between two rubber O-rings in a custom-made stainless steel filtration module, to give an effective membrane area of 2.5 cm². A 1.2 W, 365 nm ultraviolet light emitting diode (UV-LED) acquired from DigiKey Electronics, Minnesota, USA was placed underneath the module for delivering UV radiation through the membrane substrate to the TiO₂ layer. The spectral output and radiation pattern data of the LED were obtained from the product data sheet [18]. The LED has a narrow emission bandwidth and a spectral line half width of 15 nm, with the maximum power output occurring at 365 nm. The LED therefore emits most of its power in the wavelength band of interest for activating TiO₂ [19]. The beam angle of about 45° and a distance of 2 cm between the LED and the membrane allows the radiation to be spread more evenly throughout the membrane. To prevent the LED from overheating, it was connected to a microcontroller board (Arduino, Ivrea, Italy) to enable pulse width modulation. For each pulse period of 2.04 ms, the LED ON time was set at 15% of period duration, allowing cooling for 85% of the period duration. The voltage across the LED was 2.2 V and the current was reduced to 260 mA, from 300 mA. Reducing the power at which the LED operates also assists in lowering the operating temperature and prolonging the life of the LED. A quartz window was fixed in a hole made in the steel module to allow UV from the LED to pass through. The UV intensity emitted by the LED was measured by a UV irradiance meter (Photoelectric Instrument Factory of Beijing Normal University, Beijing).

Changes in TMP during filtration were recorded using a TPI 665L digital manometer from Accutherm, Melbourne, Australia. Changes in the temperature of the module were monitored through an Ulirvision TI384 infrared camera from OneTemp Pty. Ltd., Melbourne, Australia. The feed was driven through the filtration system by a QG20 positive displacement pump (Fluid Monitoring Inc., Syosset, USA). An electronic balance (FX-3000i WP, A&D Company Ltd., Seoul, South Korea) with real time monitoring software was used to measure the amount

of permeate (membrane filtrate) during the experiments. Total organic carbon (TOC) of test solutions was determined from a Shimadzu TOC-V CSH analyser. A UV-visible light spectrophotometer (HACH DR5000, USA) was used to measure specific absorbance at a wavelength of 254 nm (UV254).

2.3. Preparation of coating suspension

5 g of P25 TiO₂ powder was mixed with 60 mL deionised (DI) water for 30 minutes using a CAT Unidrive X1000 homogenizer operated at a speed of 8500 revolutions per minute (rpm). This part of coating suspension was labelled “Part A”, and it was sonicated for 20 minutes while preparing the Part B of the coating suspension. Part B was prepared by mixing 0.4 g of sodium alginate (SA) with 60 mL of deionised (DI) water for 30 minutes using the homogenizer. Care was taken to add alginate powder to water at a very slow rate to prevent it from sticking to the homogenizer blades. Part B was then added to Part A in little quantities while mixing the two parts of coating suspension with the help of the homogenizer. The mixture was further homogenized for 30 minutes at a speed of 15 000 rpm, followed by the sonication process for 30 minutes. The prepared coating suspension was transferred into a 200 mL beaker and magnetically stirred for 2 h prior to coating to maintain homogeneity.

2.4. Preparation of photocatalytic membranes

Each of the membrane substrates was sonically cleaned with a succession of 1% NaOH solution, 0.5% NaOCl and DI water for 20 minutes and then dried at 80 °C for 3 hours in a fan-forced oven. The membranes were weighed and covered with autoclave tape on the non-functional side on which a TiO₂ coating was not required. A custom made mechanical device was used to dip and withdraw the membrane at a speed of 2 cm/min. The membrane was kept in the suspension for 3 minutes before withdrawing it. After the coating procedure, the membrane was air dried for 12 hours and the autoclave tape was removed before it was heated to 450 °C at a rate of 1 °C/min in a programmable muffle furnace. The temperature was maintained at 450 °C for 2 hours, followed by cooling to room temperature at a rate of 1 °C/min. After this heat treatment process, the membranes were washed with DI water and oven dried at 80 °C for 2 h.

2.5. Characterisation of membranes

The topographical features and elemental composition of the membranes were analysed by a Field Emission Scanning Electron Microscope (FESEM) and an Energy Dispersive Spectroscopy (EDS), respectively. First, the samples were mounted on aluminium stubs with double-sided conductive carbon tape and sputter coated (60 mA for 50 seconds) with an approximately 4nm thick iridium coating using a Cressington 208HRD sputter coater. The conducting coating assists in preventing charge accumulation and obtaining clear images. After applying the coating, the samples were imaged using a Zeiss Merlin Gemini 2 FESEM instrument operated in the secondary electron (SE) mode and an accelerating voltage of 5 kV.

For element identification, the accelerating voltage was set at 15 kV and an EDS detector (80 mm² X-Max) equipped with AZTEC software (Oxford Instruments Pty Ltd) was used.

The pore size of the substrate and membrane were determined via capillary flow porometry using a Quantachrome Porometer 3 GZ series from Quantachrome Corp., Boynton Beach, FL, USA. The instrument measures the flow of nitrogen gas through the dry and wet (using a wetting liquid) membrane samples as a function of TMP and then calculates the pore size using the Washburn equation. Porofil™ from Quantachrome Corp., Boynton Beach, FL, USA was used as the wetting liquid in this study.

2.6. Filtration experiments

The membrane filtration setup which was used in this study is depicted in the schematic diagram in Figure 2. The filtration setup includes a feed tank, a positive displacement pump, membrane module, 5 solenoid valves connected to a logic controller, a pressurised tank for backwashing, a digital manometer, a retentate collection tank, a permeate collection tank placed on an electronic balance and 2 data loggers to record pressure and permeate volume. To ensure safety from UV radiation, the module was housed in a metal box on which a switch deactivated by opening the box's door was installed. Filtration was carried out in the dead-end mode at constant flux. Backwashing and filtration mode were determined by programmed opening or closing of the appropriate valves, labelled V-1 to V-5.

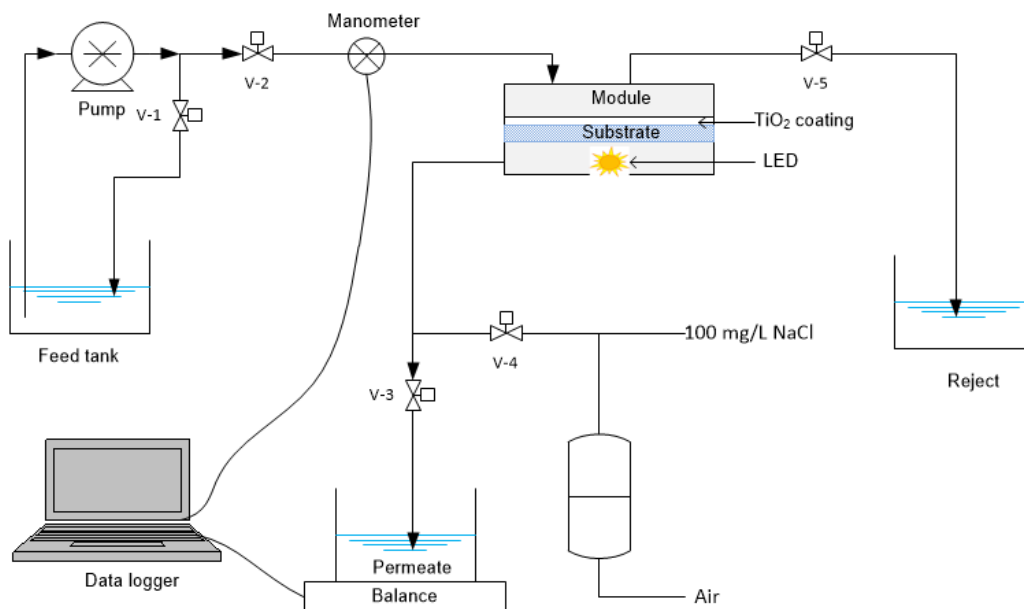


Figure 2. Schematic diagram of the filtration system used in this study.

2.6.1. Experiments with HA

Membrane filtration experiments with HA solutions were carried out at a constant permeate flux of 450 L/(m²h). The membrane was initially compacted with 20 mg/L NaCl solution for 1

hour to give a steady state pressure, followed by a 20 mg/L HA [12] and 100 mg/L NaCl solution. NaCl was added to DI water since surface and ground water systems always contain some salts. Filtration was conducted in a dead end mode in which the UV-LED was either switched ON (light) or OFF (dark) to induce the effects of photocatalysis and superhydrophilicity to alter membrane fouling, which was measured in our work through the variation of TMP. Uncoated sintered glass substrates were also used in these experiments and considered for control experiments purposes.

2.6.2. Experiments with BSA and SA

Membranes were compacted with 100 mg/L NaCl solution for 1 hour followed by a 50 mg/L solution of BSA, which also contained 5 mg/L CaCl₂ and 20 mg/L NaCl. Backwashing of the membrane was achieved by opening appropriate valves to allow 100 mg/L NaCl to flush the membrane from the permeate side at 1 hour intervals. Backwash duration was 1 minute and the pressure was set at 200 kPa. Filtration was conducted in a dead end mode in which the UV-LED was either switched ON (light) or OFF (dark). The same procedure was followed for 20 mg/L SA containing 5 mg/L CaCl₂ and 20 mg/L NaCl. The operating flux was set at 70 L/(m²h) for SA and 100 L/(m²h) for BSA. These were chosen to be above the critical flux to demonstrate a positive effect from the action of the photocatalysis as compared to when no light is applied.

2.7. Evaluation of membrane cleaning efficiency

The cleaning efficiency of the photocatalytic membranes was evaluated through the recorded trend of TMP, the hydraulic cleaning efficiency (HCE) and the hydraulically irreversible fouling index (HIFI).

HCE was determined from Equation 1, which calculates the fouling reversibility after each filtration cycle n [20]:

$$HCE = \sum_{n=1}^k \frac{HCE(n)}{k} = \frac{P_f^n - P_{ini}^{n+1}}{P_f^n - P_{ini}^n} \quad (1)$$

where P_{ini}^n and P_f^n are the initial and final TMP values of cycle n respectively, and P_{ini}^{n+1} is the initial TMP value of cycle $n+1$.

The HIFI, an indication of fouling which could not be reversed by backwashing and/or the photocatalytic effect, was calculated using Equation 2 [13]:

$$1/J_s' = 1 + (HIFI)V_s \quad (2)$$

where J_s' is the normalized specific flux, which is replaced by $(J/P_{ini})/(J/P_0) = P_0/P_{ini}$ when the filtration is carried out under constant flux. P_0 (kPa) is the TMP of fresh membrane, and P_{ini} is

the initial TMP after each backwashing event, and V_s (L/m^2) is the total volume of filtrate per unit membrane area.

The HIFI fouling index model is not attributed to a specific fouling mechanism, therefore it could be used for all fouling mechanisms such as pore narrowing/blocking and cake formation, or a combination of both [20].

If the plot of $(1/J_s')$ versus (V) is linear, i.e. the rate of increase in filtration resistance is linearly proportional to V , the HIFI can be quantified using linear regression. In instances where a linear function cannot be obtained, a 2 point method can be used to determine the HIFI. In this case, instead of using all performance data, the first and the last points are used to calculate the average rate of increase in filtration resistance [20].

2.8. Fouling mechanism

Fouling of the membrane can occur either through pore blocking or the formation of a cake layer on the surface of the membrane, leading to filtration resistance. The mechanism of fouling that occurred was determined from observing SEM images of the membranes as well as applying the resistance-in-series model.

The resistance-in-series model [21] was used to analyse and calculate the total membrane resistance (R_t), which has contributions from the intrinsic membrane resistance (R_m), resistance due to pore blocking (R_p) and resistance due to cake formation (R_c).

$$R_t = R_m + R_p + R_c \quad (3)$$

R_m and R_p make up the internal membrane resistance, R_f .

$$R_f = R_m + R_p \quad (4)$$

At constant flux, J , the resistance can be determined from Equation 5,

$$J = \frac{P}{\mu R} \quad (5)$$

where P is the TMP (Pa), μ is the solution viscosity (Pa.s) and R is either R_t , R_m or R_f , depending on the experimental conditions.

R_t can be estimated from Equation 5 by finding J and P from the filtration experiments of either using BSA or SA solution at constant flux. In this study, J and P measurements were taken at 6 hours. R_m was also obtained from Equation 5 after obtaining the results from the pure water filtration experiments. To obtain R_f , Equation 5 was applied after gently wiping the BSA or SA fouled membrane with a wet sponge and rinsing it with water to remove the cake layer, then filtering pure water through it. R_p was then calculated from Equation 4, and R_c from Equation 3 [22].

3. Results and discussion

3.1. Membrane morphology and composition

The bare sintered glass membrane which was used in this study was composed of micro-sized particles as seen from the SEM image shown in Figure 3(a). The coating procedure described in Section 2.4 resulted in the achievement of complete coverage of the membrane surface with TiO₂ nano-sized particles, as shown in Figure 3(b) and Figure 3(c). The thickness of the TiO₂ layer was about 15 μm, as shown in Figure 3 (c). A set of EDS analyses were also conducted to confirm the effectiveness of the TiO₂ coating procedure adopted in this study. From the EDS results illustrated in Figure 3(d), a 53.5 wt% of Ti on the functional side of the membrane and just 0.2 wt% silicon shows the effectiveness of the coating method in covering the surface with TiO₂, to the extent that the minor elements Na and Al, which make up borosilicate glass, were not detected. Detection of 0.2 wt% Si on the coated side could also be a result of electron penetration into the membrane layer. The bare side of the membrane had a composition of 51.6 wt% O, 35.1 wt% Si, 2.6 wt% Na and 1.1 wt% Al, confirming its silicate properties [23].

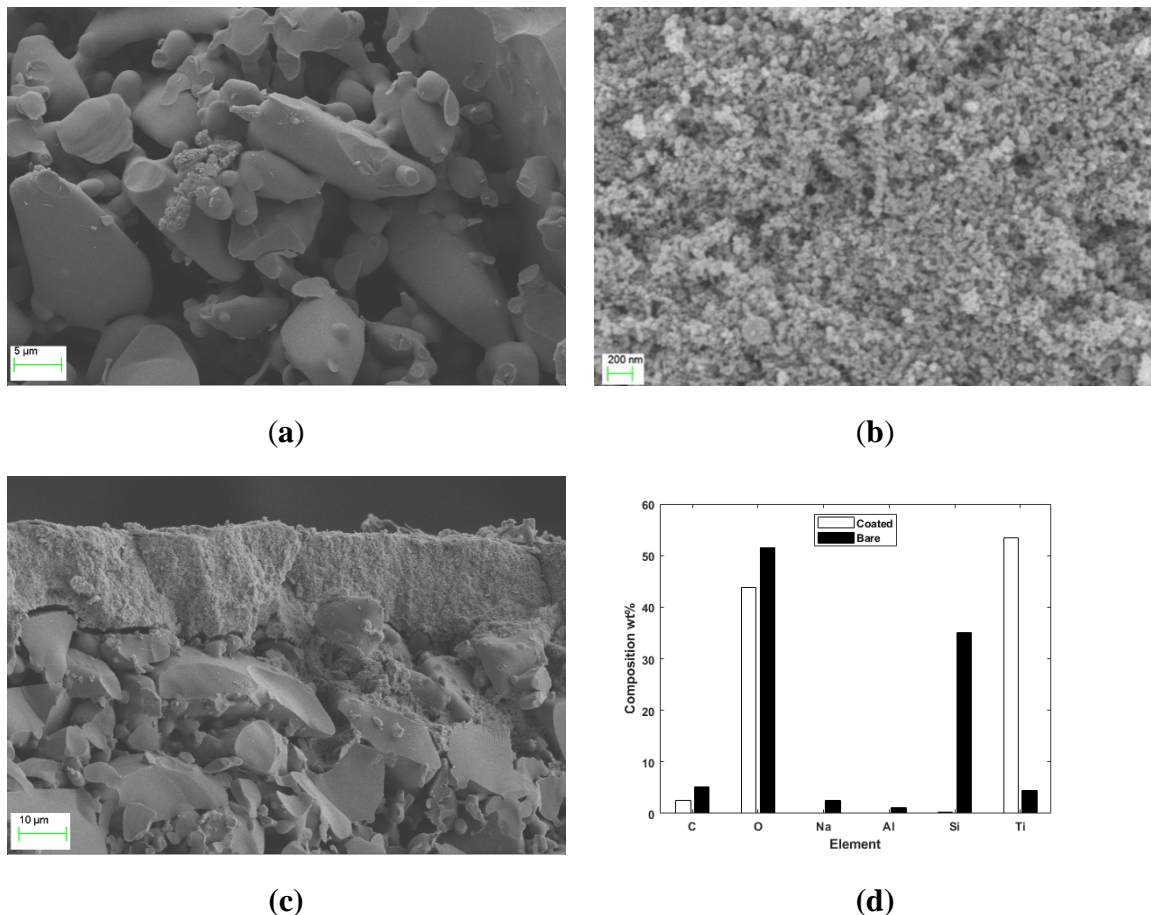


Figure 3. SEM images of the uncoated membrane surface (a), TiO₂ coated membrane surface (b) and membrane cross section (c), and EDS determined elemental composition of the coated and bare side of the membrane (d).

The membrane pore size data of the membrane determined by capillary flow porometry is shown in Table 1. The average pore size of the P25 coated membrane was 0.53 μm, which is

about a third of that of the bare porous glass substrate. The coated membrane is therefore in the MF range, meaning fouling would be expected. Despite the relatively larger pore sizes of MF membranes of more than 0.1 μm , rapid fouling by HA as high as 90% flux decline in 5 minutes for 100 mg/L HA and 50% flux decline in 5 minutes for 10 mg/L HA has been reported for MF membranes of 1.9 μm pore size [24]. Fouling is not only determined by the membrane pore size but other factors such as the operating flux or pressure, solution pH, electrostatic interaction of HA with the membrane surface and concentration. In conclusion, the MF property of the P25 coated porous glass membrane indicates its suitability for fouling investigation in this study.

Table 1. Pore size data of the membrane determined by capillary flow porometry.

Material	Mean pore size (μm)	Minimum pore size (μm)	Maximum pore size (μm)
Bare substrate	1.4	0.58	2.0
P25 coated membrane	0.53	0.18	1.0

The water permeability of the bare and P25 coated membrane was measured at a constant flux of 450 L/(m²h) and a temperature of 24 °C. Table 2 shows the water permeability results for bare and P25 coated membranes. The reduced pore size of the membrane was also apparent in the reduced pure water permeability of the coated membrane when compared to the bare membrane.

Table 2. Water permeability of the bare and coated membrane measured at a flux of 450 L/(m²h) and 24 °C.

Material	Pressure (kPa)	Permeability [L/(m²hPa)]
Bare substrate	4.5 \pm 1	0.10 \pm 0.01
P25 coated membrane	15 \pm 2	0.030 \pm 0.002

3.2. Light transmittance through the substrate

The light intensity of the UV-LED, measured from a distance of 2 cm, was 12 mW/cm². The membranes were wetted with water before intensity measurements to mimic filtration conditions. Measured through the bare membrane, the intensity was 0.45 mW/cm², and 0.10 mW/cm² through the coated membrane. The reduced transmittance on the coated membrane is due to the fact that some of the light is absorbed by the photocatalyst coating.

From these figures, it is apparent that the substrate absorbs most of the light energy. However, it has been shown that the light that transmits through the substrate is sufficient to facilitate photocatalytic reactions on the membrane surface [13]. Moreover, the intensity of 0.45 mW/cm² transmitted through the wet glass substrate is comparable to that applied in other studies that used the traditional light directing configuration. For example, 0.3 mW/cm² from visible light LEDs illuminating a nitrogen-doped titania-alumina membrane led to a 57% removal of methylene blue [25] and 0.39 mW/cm² from 365 nm LEDs illuminating titania self-assembled on porous TiO₂ sheets led to successful removal of selected estrogens [26]. In future studies, substrates with higher light transmittances could be investigated. A few examples include polylactic acid (PLA) [27], silk fibroin [28], cellulose [29-31], single-walled carbon nanotubes (SWCNTs) [32-34] and free standing graphene oxide [35].

3.3. Filtration of synthetic water containing HA

Figure 4 shows the TMP profiles under different UV lighting scenarios while filtering HA solution. Figure 4(a) shows the continuous UV ON and OFF TMP profiles in 6 hours of filtration, where only a slight increase in TMP was recorded during the filtration with HA solution when the membrane was illuminated with UV. However, TMP rapidly increased when conducting the experiment without UV illumination. Absence of fouling could be a result of two factors, namely degradation of HA and/or induced hydrophilicity, as discovered by Chen and Poon [9]. However, the degradation was very low as concluded from UV₂₅₄ absorbance and TOC tests. Only a 37% decrease in the UV₂₅₄ absorbance and an insignificant decrease in TOC of permeate stream was recorded during UV illumination. This would be expected because the low contact times with the photocatalyst could not lead to complete mineralisation of HA, or any significant degradation. Hence, the observed anti-fouling behaviour could instead be due to the induced hydrophilicity that occurs on the surface of the TiO₂ coated photocatalytic membrane [4, 9]. The hydration layer induced on the membrane surface would prevent HA from attaching to the membrane surface. HAs are known to have a high propensity of irreversibly fouling MF TiO₂ ceramic membranes [36], therefore fouling mitigation by the photocatalytic layer was quite remarkable. When the UV-LED was OFF, the induced beneficial phenomena did not occur, hence the observed TMP rise and fouling mainly due to contact of HA with the membrane, leading to pore blocking [37].

Figure 4(b) shows the case where UV ON or OFF status is alternated every two hours. In this test, when the UV was initially ON, a very low rate of increase of fouling during the first two hours occurred, being consistent with the continuous test in Figure 4(a). In the next 2 hours when the UV was OFF, fouling of membrane began to increase at a higher rate, but it significantly slowed again when UV illumination was recommenced for the last two hours. Due to low HA degradation and the fact that the irreversible internal fouling is common in MF membranes when HA is present [37], there was no significant membrane recovery when the LED was switched back to ON, but the beneficial effect of UV light on the TiO₂ surface was enough to prevent further accumulation of HA on the membrane surface.

When the filtration run commenced without UV illumination, TMP rise was very similar to the continuous test in Figure 4(a) until UV illumination began after 2 h. When illumination began, some recovery of the initial TMP occurred until the TMP rise appeared to cease. The observed recovery in TMP then stops when the rate of degradation becomes less than the rate of deposition, resulting in constant TMP. When there was no UV exposure in the last two hours, a sharp rise in TMP was recorded, demonstrating a higher rate of fouling which interestingly reached the similar TMP value after six hours when no light was used at all (Figure 4(a)). This strongly suggests that the accumulated organics over the six hour dead-end filtration with no backwash reassembles into a fouling layer of similar flow resistance as that which was made in the absence of photocatalytic activity. The photocatalytic activity appears to inhibit formation of a cohesive fouling layer. The results of this experiment confirmed the effectiveness of continuous UV exposure on to the membrane for controlling HA fouling. Providing UV illumination throughout the filtration run is therefore the most effective way of preventing HA fouling.

The findings of a previous study conducted by Zhu *et al* [4] for assessing the mitigation of membrane fouling when UV illumination is present match with the results obtained in our study. They found that photocatalytically partially oxidized humic acid (OHA) reduces the fouling propensity of polyvinylidene fluoride (PVDF) ultrafiltration membranes better compared to purified humic acid (PHA). Over a filtration duration of 140 minutes, the OHA experiment had a flux 21.3% higher than the PHA experiment. Photocatalytic oxidation facilitated the decomposition of PHA into smaller, more hydrophilic fragments. OHA became softer, weakening its adherence to the membrane and OHA-OHA interactions. Hence, in the study reported in this paper, even though mineralisation of HA did not occur, photocatalysis does change its structure, leading to less adherence to the membrane and less fouling.

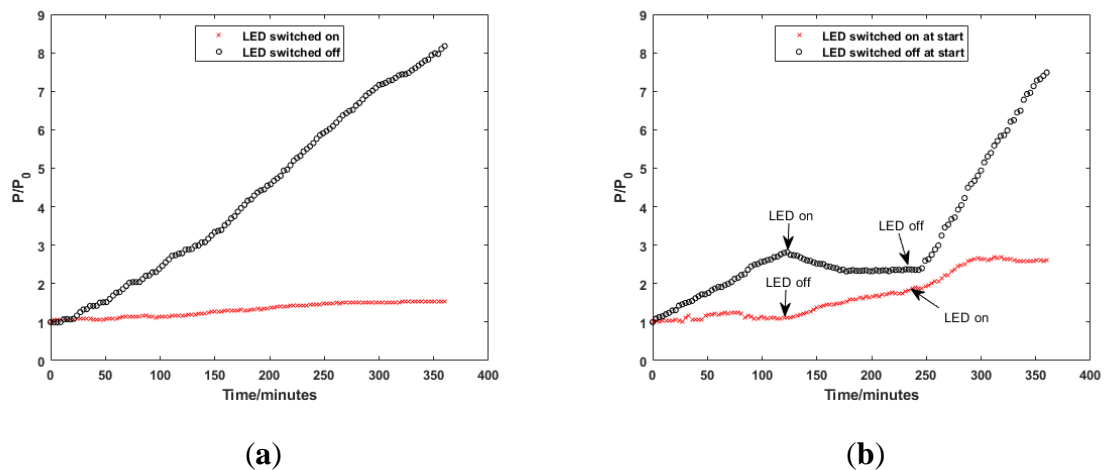
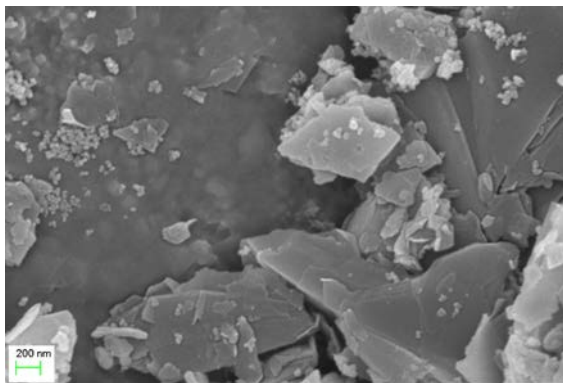


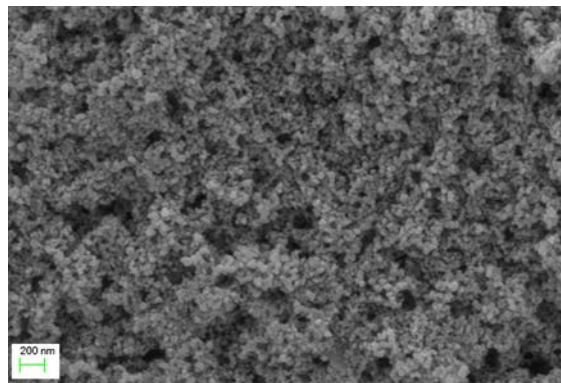
Figure 4. Normalised pressure-time profiles for HA filtration: (a) without a change of the UV-LED status and (b) when the status of the UV-LED is changed every 2 hours. P is the TMP at the selected time interval and P_0 (9.0 kPa) is the initial TMP.

3.4. Filtration of synthetic water containing BSA

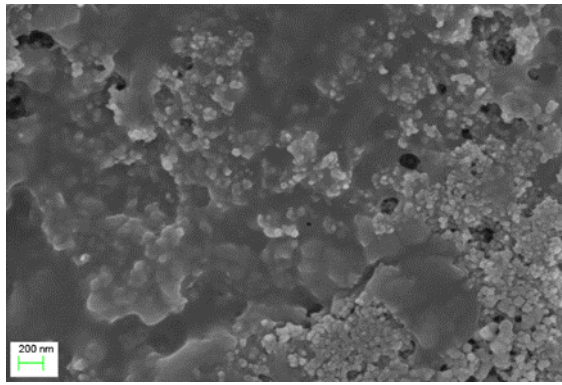
Figure 5 shows the SEM surface images of membranes fouled under different test conditions while filtering BSA solution as well as the TMP profiles and fouling layer elemental composition. Figure S3 shows a membrane cross section after filtration of BSA. There was no noticeable change in the TiO₂ layer thickness after the filtration processes. However a denser coating of about 1 μm can be seen that is likely to be the organic fouling material on the membrane surface. The SEM image shown in Figure 5 (a) shows that filtration of BSA solution with UV exposure resulted in the foulant being retained in the form of flakes on the membrane surface, leading to a 70% removal of TOC. It was found that the fouling could be easily reversed by backwashing, as the BSA flakes were loosely deposited on the membrane, resulting in better membrane restoration, as shown in Figure 5 (b). Without UV illumination, the foulant tended to penetrate pores rather than being retained on the membrane surface, as shown in Figure 5 (c). This led to poor restoration of the membrane after backwashing, as shown in Figure 5 (d). As seen in Figure 5(f), an increase of the amount of carbon deposited on the membrane from 2.5 wt% to 35.6 wt% indicates that the fouling of membrane was primarily due to organic fouling. The P25 TiO₂ coated surface largely prevented fouling of the membrane and backwashing significantly led to TMP recovery as shown in Figure 5(e) for both the photocatalytic and non-photocatalytic processes during this study. The photocatalytic process kept the operating TMP low ($P/P_0 < 10$) throughout the filtration period, compared to the TMP during the non-photocatalytic process when there was no UV ($P/P_0 < 35$). These observations could be attributed to effects of photocatalytic alteration of the protein structure as described by Xu *et al* [38] as well as induced super-hydrophilicity [9], which potentially maintained a chemisorbed layer of water on the membrane surface for as long as the UV radiation was present.



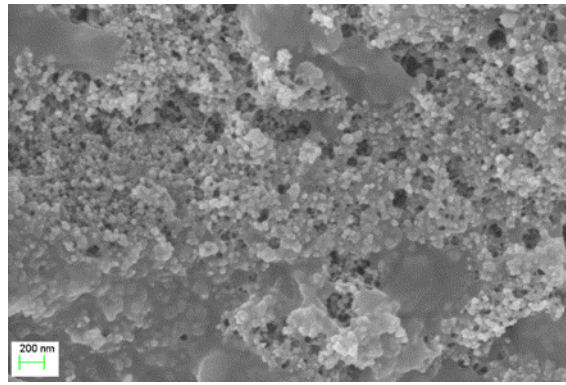
(a)



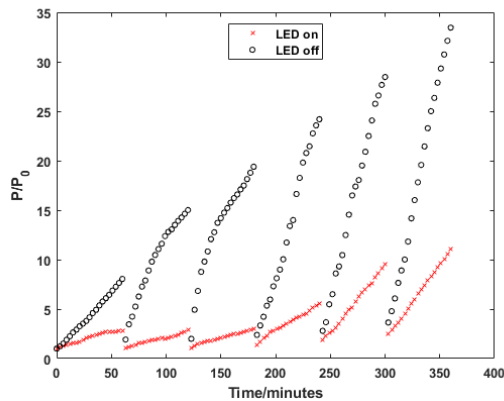
(b)



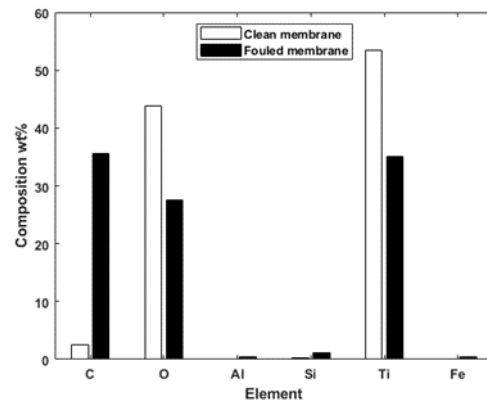
(c)



(d)



(e)



(f)

Figure 5. SEM surface images of the membrane after BSA filtration, LED on (a) before backwash (b) after backwash, and LED off (c) before backwash (d) after backwash, (e) the normalised pressure-time profiles of the filtration run and (f) elemental composition of the clean and BSA fouled membrane surface. P is the TMP at the selected time interval and P_0 (6.5 kPa) is the initial TMP.

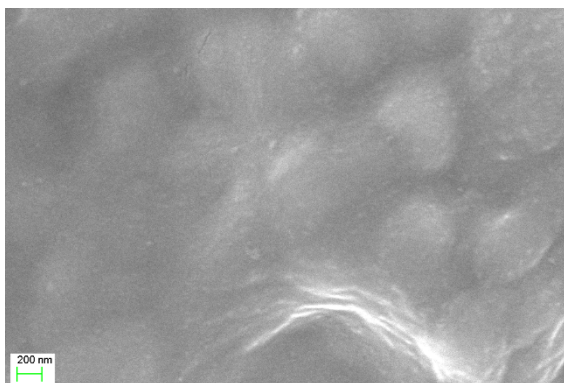
3.5. Filtration of synthetic water containing SA

Figure 6 shows the SEM surface images of membranes fouled under different test conditions while filtering SA solution as well as the TMP profiles and fouling layer elemental composition. Unlike BSA, the SEM image depicted in Figure 6(a) shows that SA was retained on the membrane surface in the form of a continuous layer during the experiments with UV exposure. Because of the chemical nature of SA as a binder, it forms complex cross-linked structures [22], preventing the complete recovery of the membrane from backwashing. Because of its larger molecular size compared to HA and BSA, an 80% reduction of TOC in the permeate stream relative to the feed was achieved. TMP profiles in Figure 6(e) show that the photocatalytic processes were still effective in keeping the operating TMP lower compared to when UV illumination was not provided. Based on elemental analysis in Figure 6(f), the deposited SA layer was thin, since the fouled membrane still showed a 40.1 wt% composition of Ti, down from 53.5 wt% of Ti in the clean membrane. Because of the thinness of the SA

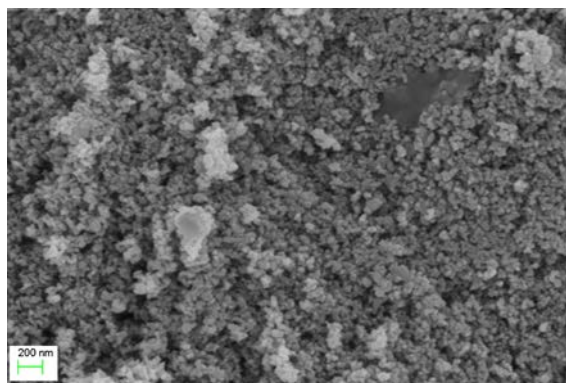
layer, electrons from EDS analysis could still penetrate it to be able to reach the titania layer beneath it. Just like with BSA, induced beneficial effects of UV light on the TiO_2 surface led to a prevention of pore blocking, which led to better membrane restoration compared to the non-illuminated experiment. Without UV illumination, significant penetration of the foulant into the pores occurred, leading to poor membrane restoration, as seen in Figure 6(d).

As shown in Figure 6 (e), UV illumination had the overall trend of decreasing both reversible and irreversible fouling since TMP rise between backwash events decreased, and the TMP returned close to the original values, respectively. However, as more fouling occurs over time, the positive effect of UV illumination also diminishes, leading to increasing fouling, as depicted by the steeper slopes of normalised pressure. Further refinement of the process could see increased backwash frequency or reduced fluxes, but regardless, there does appear to be a gradual irreversible rise in TMP even with photocatalytic action to mitigate fouling, implying the eventual (but significantly less frequent) need for a chemical clean.

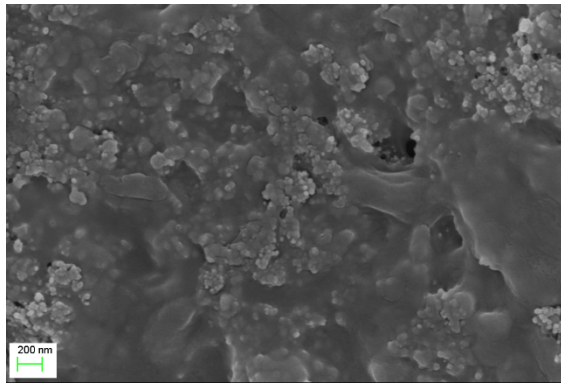
The TMP behaviour indicating fouling may also be explained by the choice of an experimentally convenient backwash solution (normally permeate is used as a backwash), being higher in NaCl concentration (100 mg/L versus 20 mg/L in the feed), and not having any Ca^{2+} ions. Ca^{2+} ions and other divalent ions are known to play an important role in SA fouling, because they preferentially bind to carboxylic groups on alginate to form a highly fouling egg-box-shaped gel network [20, 39]. An important step for reversing alginate fouling is therefore breaking the calcium-alginate complex. Na^+ ions that were present in the more concentrated backwash solution (100 mg/L NaCl) can play this role, which can break up the cross-linked alginate complex by ion exchange. Presence of Na^+ ions in the backwash solution can therefore explain the high recoveries obtained through hydraulic backwashing, even without UV illumination. Regardless of whether the relatively Na^+ rich and Ca^{2+} lean backwash solution played a role on the fouling behaviour evident as TMP, its use was consistent across all experiments (both BSA and SA), and differences can still be attributed to the impact of UV light on the TiO_2 membrane surface.



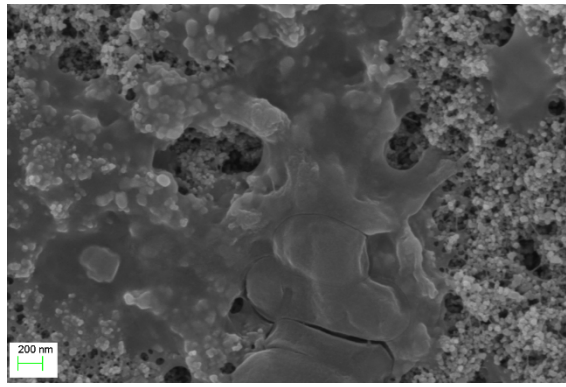
(a)



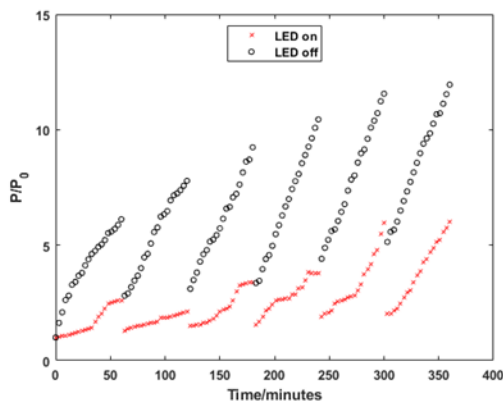
(b)



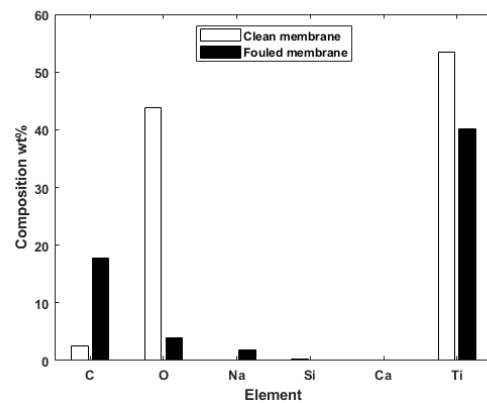
(c)



(d)



(e)



(f)

Figure 6. SEM surface images of the membrane after SA filtration, LED on (a) before backwash (b) after backwash, and LED off (c) before backwash (d) after backwash, (e) the normalised pressure-time profiles of the filtration run and (f) elemental composition of the clean and BSA fouled membrane surface. P is the TMP at the selected time interval and P_0 (3.2 kPa) is the initial TMP.

3.6. Fouling indices

The fouling indices, namely hydraulic cleaning efficiency (HCE) and hydraulically irreversible fouling index (HIFI), calculated from Equation 1 (HCE) and Equation 2 (HIFI), for BSA and SA filtration are shown in Figure 7. The HCE of the membrane was recorded above 86% for both BSA and SA. This HCE was high regardless of the state of the UV-LED, showing that the membrane was largely effective in minimising organic fouling, due to the TiO_2 coating which renders it intrinsically hydrophilic. This is consistent with other ceramic membranes due to their hydrophilic nature [40, 41]. Most significantly, the photocatalytic processes kept hydraulically irreversible fouling low, as seen by the HIFI values in Figure 7(b). For BSA and SA, the photocatalytic membrane filtration processes resulted in a reduction of HIFI by 2.7-fold and 4.2-fold respectively, compared to when conducting the experiments in UV-LED OFF mode. In comparison, as shown in Figure 7 (b), the HIFI values from natural surface water filtration through commercial single channel tubular ceramic membranes with pore sizes of

0.14 μm 0.20 μm had corresponding HIFI values of 0.0252 m^2/L (Lit 1) and 0.0297 m^2/L (Lit 2), respectively [36].

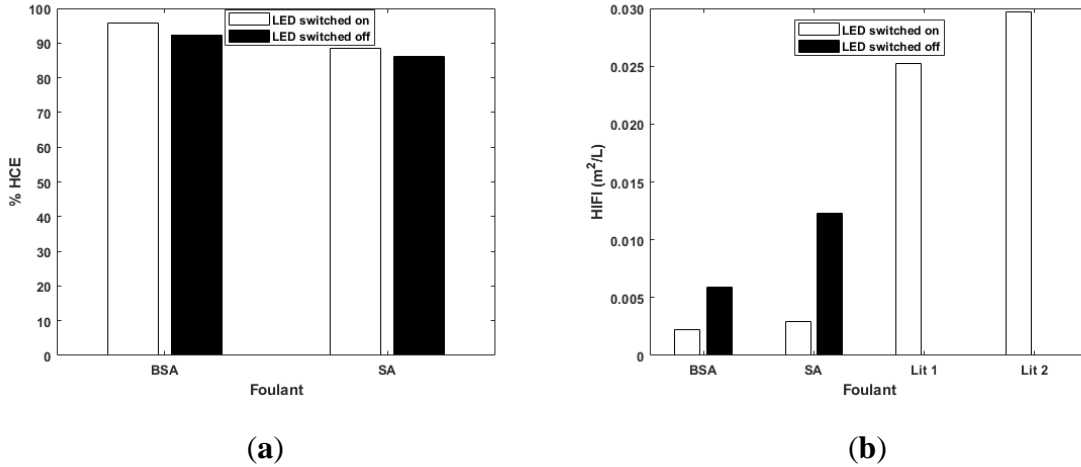


Figure 7. The fouling indices calculated for the filtration of BSA and SA (a) HCE values in this study and (b) the HIFI in this study and two selected literature values (Lit 1 and Lit 2) [36].

3.7. Fouling mechanism

The nature of the fouling that occurred on the membrane was evaluated using the resistance-in-series model, described in Section 2.8, as well as SEM images obtained for the membranes. The filtration resistance values for BSA and SA are shown in Figure 8(a) and (b) respectively. In general (regardless of UV light), the total filtration resistance (R_t) in filtering BSA solution was much greater than for SA solution, correlating to the TMP profile differences in Figure 5 and Figure 6 where BSA showed faster TMP rise rates than SA. This could be simply due to the higher concentration of BSA (50 mg/L vs 20 mg/L for SA), and/or that BSA solution filtration flux was higher (100 $\text{L}/(\text{m}^2\text{h})$) versus 70 $\text{L}/(\text{m}^2\text{h})$ for SA), selected for testing under sustainable performance conditions. The influence of UV on the fouling will therefore be analysed separately for BSA and SA solution filtration.

Considering the effect of UV-light, the results indicate that UV light directed to the photocatalytic coating on the membranes led to measureable beneficial effects to reducing membrane filtration resistance. Generally, both internal (pore blocking) and surface (cake layer formation) fouling occurred. Pore blocking and constriction is expected in MF membranes due to the presence of large pore sizes [37]. The photocatalytic processes, facilitated by the UV-LED light exposure resulted in a 3.0-fold reduction in the total filtration resistance (R_t) during BSA filtration and a 2.4-fold reduction during SA filtration. A significant reduction in the internal filtration resistance (R_f) for both BSA and SA was also recorded. The photocatalytic effect on the membrane also slightly decreased the intrinsic membrane resistance (R_m). Generally, it was found that UV-LED illumination leads to reduced pore blocking and cake layer formation during photocatalytic membrane filtration. All these observations were supported by SEM analysis of the membranes.

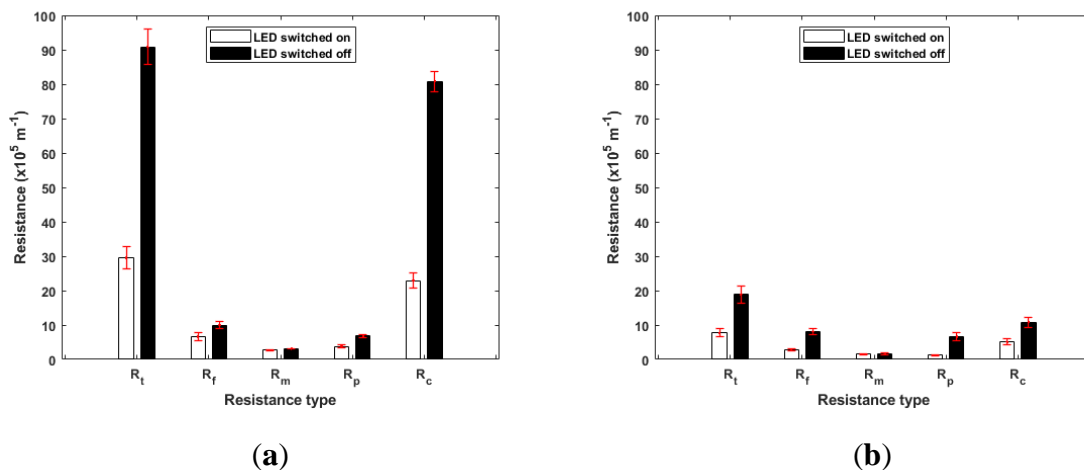


Figure 8. Filtration resistance values for the filtration of (a) BSA and (b) SA.

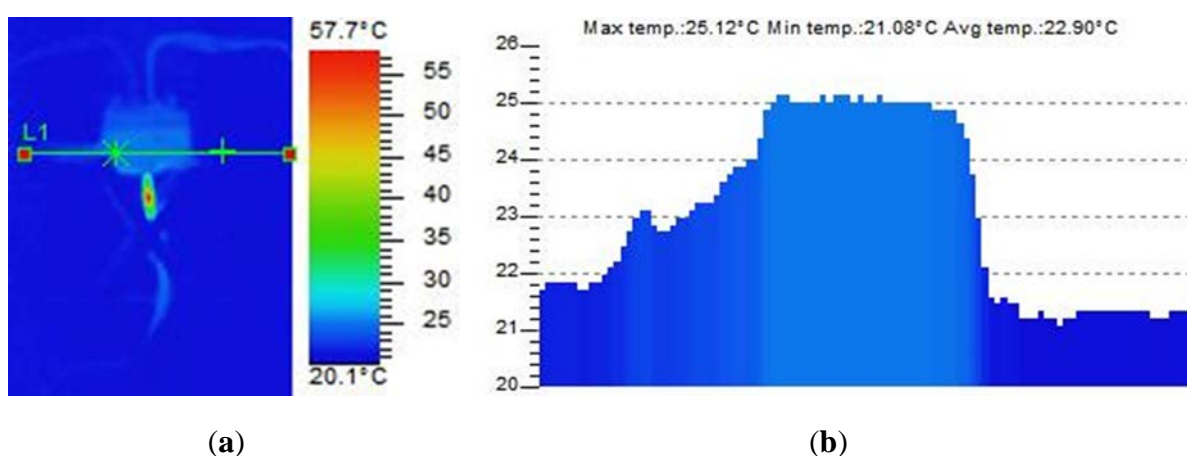
SEM analysis of the membranes at selected events during the filtration process supported the conclusions that were made from the resistance-in-series model. With UV illumination, the foulants tended to form a cake layer on the membrane surface rather than penetrate the pores. Without UV, penetration of the pores occurred, resulting in an increase in pore blocking resistance, R_p . These observations can be explained by the effect of induced hydrophilicity that occurs in the presence of UV [9]. Enhanced hydrophilicity of the membrane surface also lowers the intrinsic resistance of the membrane, R_m , while also preventing direct adsorption of the hydrophobic BSA and SA and assembly of a cohesive fouling layer. This has the net result of decreasing the observed internal filtration resistance of the membrane.

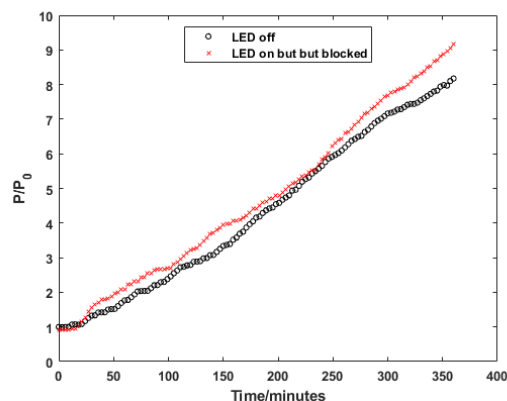
Reduction of the total filtration resistance could be explained by changes in the intermolecular interactions that occur due to photocatalytic processes facilitated by UV radiation. Polysaccharides are known to gel due to intermolecular cross-linking of the polysaccharide chains [15], while the carboxylic groups ($-\text{COOH}$) in proteins enable them to chemically bind to Ca^{2+} ions present in water, resulting in observed MF membrane fouling [37]. The crosslinking can result in the formation of complex networks which increase the effective size and dimensions of the biopolymers. However, under UV illumination, new species in the form of photo-generated electrons and holes can interfere with the crosslinking interactions. The redox potential of the electron-hole pair is greater than the competing species, therefore the hole, for example, can oxidise the carboxylic group, initiating the formation of reactive radical species which effectively lead to decomposition of biopolymer chains. Although this may not be enough to result in complete mineralisation of the organics, it is enough to prevent the formation of cross-linked complexes which increase the fouling propensity (hydraulic resistance to water flux) of the biopolymers. This could be the reason why BSA appears as flakes on the membrane surface on the SEM image. BSA (66 kDa), being of lower molecular weight than SA (120-190 kDa), would be expected to be affected more by the size reducing effect of the photocatalytic reactions.

3.8. Investigating possible thermal effects

A test was conducted to rule out the possibility that beneficial low-fouling effects could have instead been caused simply by temperature increases due to the UV-LED. Figure 9 (a) shows a thermal camera image of the membrane module with LED fitting coming from the bottom (LED fitting recorded highest temperature, indicated by the red colour). Inlet and backwash reject tubing can be seen entering the top of the module, while the permeate tubing can be seen at the lower part of the image. Line “L1” in Figure 9 (a) passes across the horizontal point where the membrane is housed in the stainless steel module. The temperature profile along this line is shown in Figure 9 (b). As shown in Figure 9 (a) and 9 (b), it was found that the temperature difference between the ambient temperature and the reactor chamber of the membrane module was only 3 °C. The LED had a heat sink which was isolated from the main module components, and hence, there was no adverse temperature increase caused by overheating of the LED which could have led to thermal energy transfer to the reactor. It is therefore unlikely that thermally induced structure changes or reactions could be the reason for the anti-fouling effects observed during the experiments reported in this article.

To further demonstrate that UV light energy was responsible for the observed low-fouling beneficial effects, another membrane filtration trial was conducted using a HA synthetic solution. The filtration process was carried out in the LED ON mode, but with the light blocked by aluminium foil. This was done to recreate the thermal conditions induced by the LED but not the conditions necessary for photocatalysis to take place. As shown in Figure 9 (c), the TMP rise was comparable to when the LED is OFF. The recreated thermal conditions were therefore not enough to explain the low-fouling effects reported earlier in this paper.





(c)

Figure 9. (a) Temperature profile of the module and surroundings, (b) temperature along the axis which passes through the reactor chamber and (c) normalised pressure-time profile of the non-photocatalytic filtration of HA. P is the TMP at the selected time interval and P_0 (9.0 kPa) is the initial TMP.

To add to these findings, future studies will look at the effect of parameters such as pH, ionic strength, contaminant concentration and flux on the membrane's anti-fouling behaviour. Also testing the membrane with real water samples is the next logical step. The induced superhydrophilicity implied from the literature could also be tested, for example by water contact angle method.

4. Conclusion

In this work, a light conducting photocatalytic membrane was fabricated and tested for application in water treatment. The light conducting substrate offered a new route through which light can be provided to the photocatalytic layer. The photocatalytic processes provided a continuous means for mitigating organic fouling during filtration, resulting in low rates of reversible and irreversible fouling of the membrane. The light conducting substrate can allow simplified integration of light sources into photocatalytic membranes, where light can be directed from the end of the membrane element and transmitted through its length. The concept could offer a sustainable, low maintenance technology that produces purified water for marginalised communities, which maintains its operation by simply exposing it to the sun.

Acknowledgements

This work was supported by the Victoria University International Postgraduate Scholarships (VUIPRS) and the Institute for Sustainable Industries and Liveable Cities (ISILC), Victoria University, Melbourne. The invaluable assistance given by Miroslav Radev and Donald Ermel in setting up the electronics for the UV-LED and workshop fabrication of the stainless steel membrane module, respectively, is greatly appreciated.

References

- [1] H. Vatankhah, C.C. Murray, J.W. Brannum, J. Vanneste, C. Bellona, Effect of pre-ozonation on nanofiltration membrane fouling during water reuse applications, *Separation and Purification Technology*, 205 (2018) 203-211.
- [2] A. Khalid, A. Abdel-Karim, M. Ali Atieh, S. Javed, G. McKay, PEG-CNTs nanocomposite PSU membranes for wastewater treatment by membrane bioreactor, *Separation and Purification Technology*, 190 (2018) 165-176.
- [3] A. Merenda, L. Kong, B. Zhu, M.C. Duke, S.R. Gray, L.F. Dumée, Functional Nanoporous Titanium Dioxide for Separation Applications: Synthesis Routes and Properties to Performance Analysis, in: M. Pannirselvam, L. Shu, G. Griffin, L. Philip, A. Natarajan, S. Hussain (Eds.) *Water Scarcity and Ways to Reduce the Impact: Management Strategies and Technologies for Zero Liquid Discharge and Future Smart Cities*, Springer International Publishing, Cham, 2019, pp. 151-186.
- [4] R. Zhu, A.J. Diaz, Y. Shen, F. Qi, X. Chang, D.P. Durkin, Y. Sun, S.D. Solares, D. Shuai, Mechanism of humic acid fouling in a photocatalytic membrane system, *Journal of Membrane Science*, 563 (2018) 531-540.
- [5] Z. Geng, X. Yang, C. Boo, S. Zhu, Y. Lu, W. Fan, M. Huo, M. Elimelech, X. Yang, Self-cleaning anti-fouling hybrid ultrafiltration membranes via side chain grafting of poly(aryl ether sulfone) and titanium dioxide, *Journal of Membrane Science*, 529 (2017) 1-10.
- [6] L. De Angelis, M.M.F. de Cortalezzi, Ceramic membrane filtration of organic compounds: Effect of concentration, pH, and mixtures interactions on fouling, *Separation and Purification Technology*, 118 (2013) 762-775.
- [7] S. Leong, A. Razmjou, K. Wang, K. Hapgood, X. Zhang, H. Wang, TiO₂ based photocatalytic membranes: A review, *Journal of Membrane Science*, 472 (2014) 167-184.
- [8] S. Banerjee, D.D. Dionysiou, S.C. Pillai, Self-cleaning applications of TiO₂ by photo-induced hydrophilicity and photocatalysis, *Applied Catalysis B: Environmental*, 176-177 (2015) 396-428.
- [9] J. Chen, C.-s. Poon, Photocatalytic construction and building materials: From fundamentals to applications, *Building and Environment*, 44 (2009) 1899-1906.
- [10] G. Matafonova, V. Batoev, Recent advances in application of UV light-emitting diodes for degrading organic pollutants in water through advanced oxidation processes: A review, *Water Research*, 132 (2018) 177-189.
- [11] B.J. Starr, V.V. Tarabara, M. Herrera-Robledo, M. Zhou, S. Roualdès, A. Ayrál, Coating porous membranes with a photocatalyst: Comparison of LbL self-assembly and plasma-enhanced CVD techniques, *Journal of Membrane Science*, 514 (2016) 340-349.
- [12] I. Horovitz, D. Avisar, M.A. Baker, R. Grilli, L. Lozzi, D. Di Camillo, H. Mamane, Carbamazepine degradation using a N-doped TiO₂ coated photocatalytic membrane reactor: Influence of physical parameters, *Journal of Hazardous Materials*, 310 (2016) 98-107.
- [13] L. Nyamutswa, B. Zhu, D. Navaratna, S. Collins, M. Duke, Proof of Concept for Light Conducting Membrane Substrate for UV-Activated Photocatalysis as an Alternative to Chemical Cleaning, *Membranes*, 8 (2018) 122.
- [14] Z. Su, T. Liu, W. Yu, X. Li, N.J.D. Graham, Coagulation of surface water: Observations on the significance of biopolymers, *Water Research*, 126 (2017) 144-152.
- [15] K. Xiao, X. Wang, X. Huang, T.D. Waite, X. Wen, Analysis of polysaccharide, protein and humic acid retention by microfiltration membranes using Thomas' dynamic adsorption model, *Journal of Membrane Science*, 342 (2009) 22-34.
- [16] L. Song, B. Zhu, S. Gray, M. Duke, S. Muthukumaran, Hybrid Processes Combining Photocatalysis and Ceramic Membrane Filtration for Degradation of Humic Acids in Saline Water, *Membranes (Basel)*, 6 (2016).
- [17] G. Plesch, M. Vargová, U.F. Vogt, M. Gorbár, K. Jesenák, Zr doped anatase supported reticulated ceramic foams for photocatalytic water purification, *Materials Research Bulletin*, 47 (2012) 1680-1686.

- [18] M. Optoelectronics, Ultraviolet Emitter MTE3650L2-UV-HP, in, 2016, pp. Product datasheet.
- [19] C. Yang, N. Han, W. Zhang, W. Wang, W. Li, B. Xia, C. Han, Z. Cui, X. Zhang, Adhesive-free in situ synthesis of a coral-like titanium dioxide@poly(phenylene sulfide) microporous membrane for visible-light photocatalysis, *Chemical Engineering Journal*, 374 (2019) 1382-1393.
- [20] H. Chang, H. Liang, F. Qu, S. Shao, H. Yu, B. Liu, W. Gao, G. Li, Role of backwash water composition in alleviating ultrafiltration membrane fouling by sodium alginate and the effectiveness of salt backwashing, *Journal of Membrane Science*, 499 (2016) 429-441.
- [21] M. Cheryan, *Ultrafiltration and microfiltration handbook*, CRC press, 1998.
- [22] S. Meng, W. Fan, X. Li, Y. Liu, D. Liang, X. Liu, Intermolecular interactions of polysaccharides in membrane fouling during microfiltration, *Water Research*, 143 (2018) 38-46.
- [23] S.L. Zakharov, Borosilicate Microporous Glasses for Reverse Osmosis, *Glass and Ceramics*, 61 (2004) 178-179.
- [24] W. Yuan, A.L. Zydney, Humic acid fouling during microfiltration, *Journal of Membrane Science*, 157 (1999) 1-12.
- [25] C.P. Athanasekou, N.G. Moustakas, S. Morales-Torres, L.M. Pastrana-Martínez, J.L. Figueiredo, J.L. Faria, A.M.T. Silva, J.M. Dona-Rodríguez, G.E. Romanos, P. Falaras, Ceramic photocatalytic membranes for water filtration under UV and visible light, *Applied Catalysis B: Environmental*, 178 (2015) 12-19.
- [26] M.J. Arlos, R. Liang, M.M. Hatat-Fraile, L.M. Bragg, N.Y. Zhou, M.R. Servos, S.A. Andrews, Photocatalytic decomposition of selected estrogens and their estrogenic activity by UV-LED irradiated TiO₂ immobilized on porous titanium sheets via thermal-chemical oxidation, *Journal of Hazardous Materials*, 318 (2016) 541-550.
- [27] W. Han, J. Ren, H. Xuan, L. Ge, Controllable degradation rates, antibacterial, free-standing and highly transparent films based on polylactic acid and chitosan, *Colloids and Surfaces A: Physicochemical and Engineering Aspects*, 541 (2018) 128-136.
- [28] G. Pasternak, Y. Yang, B.B. Santos, F. Brunello, M.M. Hanczyc, A. Motta, Regenerated silk fibroin membranes as separators for transparent microbial fuel cells, *Bioelectrochemistry*, 126 (2019) 146-155.
- [29] R. Tong, G. Chen, J. Tian, M. He, Highly transparent, weakly hydrophilic and biodegradable cellulose film for flexible electroluminescent devices, *Carbohydrate Polymers*, 227 (2020) 115366.
- [30] Z. Li, W. Liu, F. Guan, G. Li, Z. Song, D. Yu, H. Wang, H. Liu, Using cellulose fibers to fabricate transparent paper by microfibrillation, *Carbohydrate Polymers*, 214 (2019) 26-33.
- [31] D.B.K. Lim, H. Gong, Highly stretchable and transparent films based on cellulose, *Carbohydrate Polymers*, 201 (2018) 446-453.
- [32] H. Bak, S.Y. Cho, Y.S. Yun, H.-J. Jin, Electrically conductive transparent films based on nylon 6 membranes and single-walled carbon nanotubes, *Current Applied Physics*, 10 (2010) S468-S472.
- [33] O. Urper, İ. Çakmak, N. Karatepe, Fabrication of carbon nanotube transparent conductive films by vacuum filtration method, *Materials Letters*, 223 (2018) 210-214.
- [34] S. Jiang, P.-X. Hou, C. Liu, H.-M. Cheng, High-performance single-wall carbon nanotube transparent conductive films, *Journal of Materials Science & Technology*, 35 (2019) 2447-2462.
- [35] P.K. Narayanam, K. Sundararajan, Organic solvent supported fabrication of transparent free standing graphene oxide membranes, *Ceramics International*, (2019).
- [36] R. Shang, F. Vuong, J. Hu, S. Li, A.J.B. Kemperman, K. Nijmeijer, E.R. Cornelissen, S.G.J. Heijman, L.C. Rietveld, Hydraulically irreversible fouling on ceramic MF/UF membranes: Comparison of fouling indices, foulant composition and irreversible pore narrowing, *Separation and Purification Technology*, 147 (2015) 303-310.
- [37] K. Katsoufidou, S.G. Yiantsios, A.J. Karabelas, A study of ultrafiltration membrane fouling by humic acids and flux recovery by backwashing: Experiments and modeling, *Journal of Membrane Science*, 266 (2005) 40-50.
- [38] Z. Xu, T. Wu, J. Shi, K. Teng, W. Wang, M. Ma, J. Li, X. Qian, C. Li, J. Fan, Photocatalytic antifouling PVDF ultrafiltration membranes based on synergy of graphene oxide and TiO₂ for water treatment, *Journal of Membrane Science*, 520 (2016) 281-293.

- [39] P. dos Santos Araújo, G.B. Belini, G.P. Mambrini, F.M. Yamaji, W.R. Waldman, Thermal degradation of calcium and sodium alginate: A greener synthesis towards calcium oxide micro/nanoparticles, *International Journal of Biological Macromolecules*, 140 (2019) 749-760.
- [40] B. Hofs, J. Ogier, D. Vries, E.F. Beerendonk, E.R. Cornelissen, Comparison of ceramic and polymeric membrane permeability and fouling using surface water, *Separation and Purification Technology*, 79 (2011) 365-374.
- [41] M.T. Alresheedi, B. Barbeau, O.D. Basu, Comparisons of NOM fouling and cleaning of ceramic and polymeric membranes during water treatment, *Separation and Purification Technology*, 209 (2019) 452-460.